Int J Mech Mater Des (2025) 21:1643–1667
https://doi.org/10.1007/s10999-025-09796-y

Optimum design of liquefied petroleum gas (LPG) composite hybrid and non-hybrid cylinders by genetic algorithm for maximum failure pressure

Brahim Mouchane · Süleyman Baştürk

Received: 14 February 2025 / Accepted: 23 May 2025 / Published online: 12 June 2025
© The Author(s) 2025

Abstract Optimizing the design of composite cylinders is crucial for balancing structural integrity, weight reduction, and cost-effectiveness, especially with the widespread use of fiber-reinforced materials in many engineering applications. This study presents a novel approach using Genetic Algorithms to optimize liquefied petroleum gas (LPG) composite cylinders for maximum failure pressure by MATLAB software. Inspired by natural selection, the Genetic Algorithm efficiently explores design variations, considering different materials and cylinder geometries. The main goal of this study is to find the best ply angle and stacking sequence to maximize failure pressure for hybrid and non-hybrid composite cylinders. The maximum stress and Tsai–Wu criteria are used together to predict failure. The algorithm converges towards an optimal design through iterative generations, evaluated using fitness functions based on classical laminate theory. The results demonstrate the effectiveness of this approach in achieving an optimal design under mechanical and thermal loads. The optimization process exhibits strong sensitivity to the selected failure criterion, with the Tsai-Wu and Maximum Stress theories generating fundamentally different optimal configurations. For example, design I under mechanical loads, the Tsai-Wu failure criterion based GA finds that the optimal solution for carbon epoxy is $[-89/-50/56/-50/-51/-50_3/56_3/-50/56/-50/57/-50_2/56_5/57/-50_2/56]_s$. In contrast, for the maximum stress failure criterion based GA, the optimal solution is $[51_2/-50/51_2/-50_2/51/-50/51/-50/52_2/-50_2/52_3/-50_2/52/-50/51/-50_3]_s$. The analysis under combined mechanical and thermal loading highlights significant performance constraints driven by temperature variations, uncovering distinct operational regimes. Within a limited thermal range, several viable stacking sequences are achievable; however, outside this window, only simplified—yet less optimal—designs remain feasible. For example, carbon epoxy, both GA identified that $[90_{26}]_s$ is the optimal configuration. Numerical findings provide insights for hybrid and non-hybrid composite cylinders, assessing the best design based on cylinder structural efficiency and the cylinder cost.

Keywords Composite cylinder · Liquefied petroleum gas · Optimum design · Genetic algorithm · Failure pressure

1 Introduction

Liquefied petroleum gas (LPG) has become a versatile fuel source widely utilized in heating, cooking, and transportation. However, efficient storage and transportation of LPG require well-designed

B. Mouchane · S. Baştürk (✉)
Altınbaş University, Istanbul, Turkey
e-mail: suleyman.basturk@altinbas.edu.tr

B. Mouchane
e-mail: brahim24mouchane@gmail.com

containers. While commonly used, traditional metal cylinders are heavy and have safety limitations. Chandrakar et al. (2017) demonstrated that composite LPG cylinders are 54.5% lighter than steel ones, offering enhanced safety, corrosion resistance, and a "leak before fail" design. The advent of composite materials has opened up new possibilities for improving the performance and functionality of LPG storage. Fiber-reinforced composite materials offer numerous advantages. Integrating fibers into a matrix creates distinct interfaces, allowing for a unique combination of properties. Typically, fibers bear the primary load, while the matrix provides support, facilitates load transfer, and protects against environmental factors like heat and humidity. Despite the emphasis on fibers, the matrix plays a crucial role in enhancing the material's overall performance and durability (Mallick 2008). Recently, Thomas et al. (2025) demonstrated the development of sustainable epoxy composites reinforced with anisotropic, lignin-derived carbon aerogels, achieving notable improvements in dynamic mechanical properties through a simple, green processing route involving ice-templating and carbonization Incorporating generative artificial intelligence (AI) into composite material design has emerged as a transformative approach, enabling the development of innovative structures with optimized performance characteristics Hwang (2025) underscores the transformative potential of generative artificial intelligence (AI) in the design of composite materials and structures. By leveraging generative AI techniques, the study highlights advancements in optimizing composite designs, addressing challenges such as anisotropy and fracture behavior, and enhancing the overall efficiency and innovation in composite structure development. Given the complexity of composite structures, particularly in layered configurations, advanced modeling approaches are essential to accurately predict their mechanical behavior. Saidi et al. (2024) developed a refined four-variable shear deformation model to analyze the vibrational behavior of porous laminated composite plates, providing insights into how porosity distributions and structural parameters affect their dynamic responses. Belbachir et al. (2025) and Nedri et al. (2014) developed refined shear deformation theories with four unknowns, which eliminated the need for shear correction factors. However, Belbachir et al. (2025) extended their model to analyze both buckling and free vibration of cross-ply laminated plates on Pasternak foundations, while Nedri et al. (2014) focused solely on free vibration analysis using a hyperbolic shear deformation theory for laminated plates on Winkler and Pasternak foundations. Addou et al. (2024) analyzed the flexural and vibrational behaviors of laminated composite shells with varying porosity distributions using a novel sinusoidal higher-order shear deformation theory (HSDT). Similarly, Mouaici et al. (2016) investigated the vibrational characteristics of functionally graded plates with porosity employing a hyperbolic shear deformation theory. While both studies address the impact of porosity on composite structures, Addou et al. (2024) work extends the analysis to shell geometries and introduces a sinusoidal shear function, offering enhanced precision in modeling shear stress distributions. Attia et al. (2024) emphasize shell geometries and employ a four-variable shear deformation to validate the influence of curvature and boundary conditions on natural frequencies through finite element analysis. In contrast, Youzera et al. (2022) delve into plate structures with viscoelastic cores, focusing on nonlinear damping effects using harmonic balance and Galerkin methods. Highlighting the effects of geometric nonlinearity and viscoelastic damping on frequency response.

Composite LPG cylinders are generally divided into five primary categories, labeled sequentially from Type I to Type V, with differences in cost, weight, and composition. Nevertheless, the most advanced pressure vessel technology currently available is Type V, which is a composite, linerless cylinder made entirely of fiber-reinforced materials, offering maximum weight reduction and high-pressure resistance, corrosion resistance, and improved visibility for monitoring gas levels (Air et al. 2023). Few examples in the literature of Type V vessels are accessible. Jones et al. (2003) produced a Type V tank using filament winding and analyzed it with a proof test of 41.4 bar. Mallick et al. (2010) utilized a novel epoxy resin toughened system to develop several Type V filament wound Tanks. Compared to the baseline aluminium tank, one design achieved a weight reduction of 25% and an increase of 15% in the internal volume. Recent advancements in the design and testing of composite pressure vessels have demonstrated the effectiveness of numerical modeling in accurately predicting burst pressure and failure mechanisms. For instance, Mikroni et al. (2024) developed and validated a numerical

model for a Type V composite pressure vessel, achieving less than 3% deviation between predicted and experimental burst pressures. However, optimizing these cylinders requires achieving a configuration that meets safety standards while minimizing weight and preserving structural integrity. Optimizing LPG composite cylinders is crucial, not only for improving safety and efficiency but also for cutting costs and for streamlining manufacturing processes. By achieving an optimal design, manufacturers can minimize material wastage, improve production turnaround times, and ultimately offer more competitive pricing to consumers. Additionally, implementing efficient optimization techniques can drive progress in manufacturing technology, opening the door to faster and more cost-effective production methods in the future. Dedicating resources to optimizing LPG composite cylinders offers long-term benefits for producers and consumers.

In the realm of weight optimization, Akbulut and Sonmez (2011) optimized laminated composite plates across diverse loading conditions. They propose a new variant of the simulated annealing algorithm to optimize the layup design, considering fiber orientation angle and the number of plies as design variables. Predicting failure using both maximum stress and Tsai-Wu criteria, they show that their methodology can find globally optimum laminate designs, even with numerous design variables. Pelletier and Vel (2006) conducted a tri-objective optimization of a pressure vessel to maximize hoop rigidity and failure pressure while minimizing mass. Their approach utilized an integer-coded genetic algorithm for multi-objective optimization of laminated composite materials. Their results demonstrate the effectiveness of this methodology in achieving multi-objective optimization goals. They propose integrating this approach with advanced analytic or numeric laminate analysis techniques and leveraging enhanced computational resources. Engineers can benefit from a valuable tool for designing superior laminated composite structures.

Numerous studies have optimized composite structures to maximize buckling load. For example; Riche and Haftka (1993) and Nagendra et al. (1992) optimized the stacking sequence of composite plates to maximize the buckling load. Rao and Lakshmi (2009) explore the application of the Shuffled Frog-Leaping Algorithm (SFLA) for optimizing laminate stacking sequences in composite structures. They propose a hybrid version of SFLA, integrating a customized neighborhood search algorithm, adaptive search factor, and strategic crossover operator to enhance computational efficiency and reliability. Through numerical experiments, they demonstrate the efficacy of the hybrid SFLA in optimizing buckling and failure load in composite plates and designing stiffened composite cylindrical shells, outperforming other meta-heuristic algorithms like genetic algorithms. Chen et al. (2022) investigated a Bayesian optimization approach for a composite cylinder shell, utilizing a Gaussian process prior model for function representation and an acquisition function targeting the maximization of eigenvalue buckling load. The study successfully identifies optimal results for a composite cylinder with specified dimensions and a symmetric stacking sequence. This methodology demonstrates adaptability in designing complex composite structures under various conditions. Blom et al. (2010) optimized a composite cylinder for enhanced resistance to buckling under pure bending. They manipulated fiber placement techniques to vary stiffness circumferentially, ensuring manufacturability with imposed constraints. Criteria included maintaining overall stiffness comparable to a baseline laminate and exceeding specified thresholds for equivalent stiffness. The study utilized laminates of constant thickness, employing a surrogate model to minimize finite element analyses and achieving significant load-carrying capacity improvements through adjustments in fiber orientation and load path. Chattopadhyay and Ferreira (1993) analyzed the failure behavior of cylinders under axial compressive loading. They utilized design optimization and sensitivity analysis to evaluate thin-walled cylinders made from symmetric orthotropic laminates with varying wall thicknesses. Formal optimization techniques were applied to adjust diameter and ply orientations, aiming to maximize critical buckling load while imposing constraints on ply stresses. The optimization process used nonlinear programming with a two-point exponential approximation method to improve computational efficiency.

The genetic algorithm concept is attributed to John Holland at the University of Michigan in the 1970s. Holland aimed to apply principles of natural selection to artificial systems, diverging from reasoning-based systems. Implemented through computer software, these artificial systems find wide applications in

design, optimization, and machine learning domains (Soremekun 1997). From the literature review, it's evident that many studies employ genetic algorithms to solve optimization problems. For example, Liu et al. (2000) developed a permutation genetic algorithm specifically for optimizing the stacking sequence of composite laminates to maximize buckling load. Their study demonstrated that permutation GAs are more efficient than standard GAs for this type of combinatorial optimization problem, significantly reducing computational costs through effective repair strategies. Pan et al. (2021) introduced an adaptive surrogate-based harmony search algorithm (ASBHSA) for the design optimization of variable stiffness composites (VSCs). Their approach effectively addresses the challenges posed by the high nonconvexity of the design space, significantly improving optimization efficiency and performance under various loading and boundary conditions. Mallikarjun et al. (2018) used genetic algorithms to enhance the effective utilization of the tailoring capabilities inherent in filament wound cylinders by optimizing their stacking sequence. Pelletier and Vel (2006) employed a genetic algorithm to optimize a pressure vessel for maximum hoop rigidity and failure pressure while minimizing mass using a tri-objective approach. Soremekun et al. (2001) studied various elitist approaches for designing composite laminates to improve the bending/twisting coupling of a laminated cantilever beam. Messager et al. (2002) employed an analytical model of shell buckling in conjunction with a genetic algorithm to discover the optimal stacking sequences for deep submarine exploration housings and autonomous underwater vehicles.

Despite the growing interest in composite pressure vessels, a comprehensive optimization framework that simultaneously addresses mechanical and thermal loading, multiple failure criteria, and cost-effectiveness—particularly for both hybrid and non-hybrid LPG composite cylinders—remains largely underexplored. Existing studies often limit their focus to single-material configurations, neglect thermal effects, or rely on a single failure criterion, thereby restricting their applicability in real-world environments. Moreover, few works enforce material composition constraints to preserve true hybrid behavior or incorporate economic considerations within the design process. To bridge this gap, the present study proposes an enhanced genetic algorithm (GA)-based optimization methodology tailored for the design of Type V LPG composite pressure vessels. The technological objective is to maximize structural efficiency while evaluating the performance of optimized stacking sequences and ply orientations under mechanical and combined thermomechanical loading conditions. The optimization process utilizes both Tsai–Wu and maximum stress failure criteria to ensure reliable failure prediction and robustness. Three distinct laminate configurations are examined: a single-material layup, a two-material hybrid, and a three-material hybrid, each subjected to GA-based optimization. To improve convergence and maintain solution diversity, the GA is augmented with advanced operators including rank-based roulette wheel selection, cross-average crossover, and low-probability mutation. The optimization process exhibits strong sensitivity to the selected failure criterion, with the Tsai-Wu and Maximum Stress theories generating fundamentally different optimal configurations. For example, design I under mechanical loads, the Tsai-Wu failure criterion based GA finds that the optimal solution for carbon epoxy is $[-89/-50/56/-50/-51/-50_3/56_3/-50/56/-50/57/-50_2/56_5/57/-50_2/56]_s$. In contrast, for the maximum stress failure criterion based GA, the optimal solution is $[51_2/-50/51_2/-50_2/51/-50/51/-50/52_2/-50_2/52_3/-50_2/52/-50/51/-50_3]_s$. These enhancements enable effective navigation of complex, high-dimensional design spaces and prevent premature convergence. Furthermore, the integration of classical laminate theory with cost modeling allows for the identification of structurally efficient and economically viable solutions. The proposed approach demonstrates strong adaptability to varying thermal conditions and material combinations, offering a scalable and computationally efficient tool for the optimal design of advanced composite pressure vessels.

2 Modelling structure

In this study, several implicit modeling assumptions are made to simplify the analysis of the composite cylinder. The first assumption involves the thin-walled cylinder approximation, where the composite cylinder is subjected to internal pressure, with the thickness considered small relative to its radius. In this context, we further assume the absence of shear stresses in the wall, implying that the stress state is purely

normal. Additionally, uniformity of longitudinal and hoop stresses throughout the wall, indicating that these stresses are uniformly distributed along both the length and the circumference of the cylinder, have been assumed. Radial stresses are considered negligible, as they act normal to the curved plane of the isolated element and have minimal effect on the overall stress distribution. When the thin-walled cylinder undergoes internal pressure, it induces two mutually perpendicular principal stresses: namely, the hoop stress (circumferential stress) and the longitudinal stress (axial stress). Furthermore, the laminate is assumed to be symmetric, with symmetry about its mid-plane, which leads to uniform material properties across the laminate and simplifies the analysis. The analysis of the composite laminate is conducted under the plane stress condition, utilizing classical laminate theory, which is a suitable approach for laminates where the thickness is much smaller than the in-plane dimensions. Additionally, bending-extension coupling is neglected (i.e., the B matrix is assumed to be zero), a consequence of the symmetric laminate configuration, which further reduces the complexity of the analysis. Finally, the material properties are treated as constant throughout the analysis, with no consideration for aging, creep, or other time-dependent phenomena, given that the material data is directly applied without any modifications over time. These assumptions facilitate the analytical approach but limit the generality of the results to cases where such idealizations hold.

Explore a thin-walled composite cylinder subjected to internal pressure P with thickness t, an internal diameter d, and length L. Consider half of this cylinder and delve into a rectangular segment of this cylinder crafted from orthotropic layers tightly bonded together and reinforced by continuous fibers. The structure exhibits symmetry about its mid-plane. Applying internal pressure on a thin-walled cylinder generates two perpendicular principal stresses within its material.

The circumferential (hoop) stress σ_H and the longitudinal stress σ_L are as follows:

$$\sigma_H = \frac{pd}{2t} \tag{1}$$

$$\sigma_L = \frac{pd}{4t} \tag{2}$$

The resultant loads per length due to stresses in the cylinder manifest in both the hoop and axial directions are as follows:

$$N_\theta = \frac{pd}{2} \tag{3}$$

$$N_L = \frac{pd}{4} \tag{4}$$

These resultant forces correspond to in-plane normal loading, exerted within the rectangular part of the cylinder, and will be treated as a laminate plate, denoted as N_{xx} and N_{yy}

Where:

$$N_{xx} = N_L \tag{5}$$

$$N_{yy} = N_\theta \tag{6}$$

2.1 Macro-mechanical analysis of laminates

The macro-mechanical analysis of laminates was conducted using classical laminate theory (e.g. see (Kaw 2006; Tsai 1966)). The initial step in commencing the analysis involves defining the constitutive equations that link stresses to the mid-surface strains and curvatures in the global x, y, and z coordinate system for each lamina as follows:

$$\begin{bmatrix} \sigma_{xx} \\ \sigma_{yy} \\ \tau_{xy} \end{bmatrix} = \begin{bmatrix} \overline{Q_{11}Q_{12}Q_{16}} \\ \overline{Q_{12}Q_{22}Q_{26}} \\ \overline{Q_{16}Q_{26}Q_{66}} \end{bmatrix} \begin{bmatrix} \varepsilon^{\circ}_{xx} + zk^{\circ}_{x} \\ \varepsilon^{\circ}_{yy} + zk^{\circ}_{y} \\ \gamma^{\circ}_{xy} + zk^{\circ}_{xy} \end{bmatrix} \tag{7}$$

where $\overline{Q_{ij}}$ is the off-axis reduced stiffness matrix coefficients of the lamina, and k°_{x},k°_{y} and k°_{xy} are the cvatures (Hyer and White 2009).

Due to the varying stresses across different plies within a laminated composite, it is practical to introduce the concept of laminate force and moment resultants. These resultants represent the cumulative effects of stresses and moments acting on a cross-sectional area of the laminate (Chawla 1998). Defined as follows:

$$[N] = \int_{-h/2}^{h/2} [\sigma] dz \tag{8}$$

$$[M] = \int_{-h/2}^{h/2} [\sigma] z dz \tag{9}$$

By substituting Eq. (7) into Eqs. (8) and (9), the matrices that connect the force and moment resultants to the mid-surface strains and curvatures are derived.

$$[N] = [A]\left[\varepsilon^{\circ}\right] + [B][K] \tag{10}$$

$$[\mathrm{M}] = [\mathrm{B}]\left[\varepsilon^{\circ}\right] + [\mathrm{D}][\mathrm{K}] \tag{11}$$

where A is the extensional stiffness matrix, B the bending-extensional coupling stiffness matrix, and D the bending stiffness matrix, the ABD matrix component with $i, j = 1,2,6$ are the following:

$$A_{ij} = \sum_{\mathrm{k}=1}^{\mathrm{n}} \left(\overline{Q_{ij}}\right)\left(h_k - h_{k-1}\right) \tag{12}$$

$$B_{ij} = \frac{1}{2}\sum_{k=1}^{n} \left(\overline{Q_{ij}}\right)\left(h_k^2 - h_{k-1}^2\right) \tag{13}$$

$$D_{ij} = \frac{1}{3}\sum_{k=1}^{n} \left(\overline{Q_{ij}}\right)\left(h_k^3 - h_{k-1}^3\right) \tag{14}$$

To calculate mid-plane strains, both sides of Eq. (10) are multiplied by the inverse of the A matrix, and since our composite laminate in this study is symmetrical, the B matrix is equal to zero and curvatures do not exist due to symmetry and loading type.

$$\left[\varepsilon^{\circ}\right] = [A]^{-1}[N] \tag{15}$$

$$[\epsilon] = \left[\epsilon^{\circ}\right] + z[k] \tag{16}$$

$$\begin{bmatrix} \varepsilon_x^{\circ} \\ \varepsilon_y^{\circ} \\ \gamma_{xy}^{\circ} \end{bmatrix} = \begin{bmatrix} \varepsilon_x^{\circ} \\ \varepsilon_y^{\circ} \\ \gamma_{xy}^{\circ} \end{bmatrix} \tag{17}$$

Finally, local stresses can be expressed in terms of global strains as:

$$\begin{bmatrix} \sigma_1 \\ \sigma_2 \\ \frac{\tau_{xy}}{2} \end{bmatrix}_K = [T]_K \begin{bmatrix} \overline{Q_{11}Q_{12}Q_{16}} \\ \overline{Q_{12}Q_{22}Q_{26}} \\ \overline{Q_{16}Q_{26}Q_{66}} \end{bmatrix}_K \begin{bmatrix} \varepsilon_x \\ \varepsilon_y \\ \frac{\gamma_x}{2} \end{bmatrix}_K \tag{18}$$

where

$$[T] = \begin{bmatrix} \mathrm{c}^2 \mathrm{s}^2 2cs \\ \mathrm{s}^2\mathrm{c}^2 - 2cs \\ -cs\mathrm{c}s\mathrm{c}^2 - \mathrm{s}^2 \end{bmatrix} \tag{19}$$

where $\mathrm{s} = \sin\theta, \mathrm{c} = \cos\theta$, and θ is the ply angle.

2.2 Hygrothermal analysis of laminates

In simplified one-dimensional scenarios, the thermal and hygrothermal strain is assumed to be given by the following formula:

$$\varepsilon_i^T = \alpha_i\left(T - T_0\right) = \alpha_i \Delta T \tag{20}$$

$$\varepsilon_i^H = \beta_i\left(c - c_0\right) = \beta_i \Delta c \tag{21}$$

where $i = 1,2,3$, α_i is the coefficient of thermal expansion, T is the actual temperature, T_0 is the reference temperature, c_0 is the initial moisture concentration, and β_i is coefficient of moisture expansion. The coefficients of thermal expansion for an orthotropic lamina, where the fibers are oriented at an angle θ to the x direction, are provided as follows:

$$\begin{bmatrix} \alpha_x \\ \beta_x \end{bmatrix} = \begin{bmatrix} \alpha_1\alpha_2 \\ \beta_1\beta_2 \end{bmatrix} \begin{bmatrix} \cos\theta^2 \\ \sin\theta^2 \end{bmatrix} \tag{22}$$

$$\begin{bmatrix} \alpha_y \\ \beta_y \end{bmatrix} = \begin{bmatrix} \alpha_2\alpha_1 \\ \beta_2\beta_1 \end{bmatrix} \begin{bmatrix} \cos\theta^2 \\ \sin\theta^2 \end{bmatrix} \tag{23}$$

$$\begin{bmatrix} \alpha_{xy} \\ \beta_{xy} \end{bmatrix} = \begin{bmatrix} 2(\alpha_1 - \alpha_2) \\ 2\left(\beta_1 - \beta_2\right) \end{bmatrix} \begin{bmatrix} \cos\theta^2 \sin\theta^2 \\ 0 \end{bmatrix} \tag{24}$$

By definition, the total strain in the lamina is the sum of the mechanical strain and the hygrothermal strain, indeed, the mechanical strain in the lamina can be determined by subtracting the hygrothermal strain from the total strain. The constitutive Equation can be written in matrix form as:

$$\left[\varepsilon^M\right] = \left[\varepsilon^{\circ}\right] + z[k] - [\alpha]\Delta T - [\beta]\Delta c \tag{25}$$

The mechanical stresses can be calculated using the following formula:

$$\left[\sigma^M\right] = \left[\overline{Q}\right]\left(\left[\varepsilon^{\circ}\right] + z[k] - [\alpha]\Delta T - [\beta]\Delta c\right) \tag{26}$$

Substituting (26) in the integrals (8) and (9) we find:

$$\begin{bmatrix} N \\ M \end{bmatrix} = \begin{bmatrix} AB \\ BD \end{bmatrix} \begin{bmatrix} \varepsilon^{\circ} \\ K \end{bmatrix} - \begin{bmatrix} N^T \\ M^T \end{bmatrix} - \begin{bmatrix} N^H \\ M^H \end{bmatrix} \tag{27}$$

If no external loads are applied, the resultant forces N and moments M are such that N=0 and M=0 (hygrothermal loads are self-equilibrated). The thermal loads induced by the temperature difference are obtained as:

$$\begin{bmatrix} AB \\ BD \end{bmatrix} \begin{bmatrix} \varepsilon^{\circ N} \\ K^N \end{bmatrix} = \begin{bmatrix} N^T \\ M^T \end{bmatrix} + \begin{bmatrix} N^H \\ M^H \end{bmatrix} \tag{28}$$

where

$$\left[N^T\right] = \Delta T \sum_{k=1}^{n} \left[\overline{Q}\right]_k [\alpha]_K (h_k - h_{k-1}) \tag{29}$$

$$\left[N^H\right] = \Delta c \sum_{k=1}^{n} \left[\overline{Q}\right]_k [\beta]_K \left(h_k - h_{k-1}\right) \tag{30}$$

$$\left[M^T\right] = \frac{\Delta T}{2} \sum_{k=1}^{n} \left[\overline{Q}\right]_k [\alpha]_K \left(h_k^2 - h_{k-1}^2\right) \tag{31}$$

$$\left[M^H\right] = \frac{\Delta c}{2} \sum_{k=1}^{n} \left[\overline{Q}\right]_k [\beta]_K \left(h_k^2 - h_{k-1}^2\right) \tag{32}$$

To calculate mid-plane strains, both sides of Eq. (28) are multiplied by the inverse of the A matrix, and since our composite laminate in this study is symmetrical, the B matrix is equal to zero. Curvatures don't exist due to symmetry and loading type; the non-mechanical strains of the laminate corresponding to the stress resultants mentioned above can be derived from Eq. (33) as:

$$\left[\varepsilon^{oN}\right] = [A]^{-1} \left(\left[N^T\right] + \left[N^H\right]\right) \tag{33}$$

Finally, it's crucial to differentiate between the hygrothermal strains within the individual layers, denoted as $\varepsilon^{\circ N}$, and the free expansion strains, represented as ε^T, of each layer. We can calculate the local residual stresses in each layer of the laminate.

$$\left[\varepsilon^R\right]_K = \left[\varepsilon^{\circ N}\right] - \left(\left[\varepsilon^T\right]_K + \left[\varepsilon^H\right]_K\right) \tag{34}$$

$$\begin{bmatrix} \sigma_1^R \\ \sigma_2^R \\ \frac{\tau_{12}^R}{2} \end{bmatrix}_K = [T]_K \begin{bmatrix} \overline{Q_{11}Q_{12}Q_{16}} \\ \overline{Q_{12}Q_{22}Q_{26}} \\ \overline{Q_{16}Q_{26}Q_{66}} \end{bmatrix}_K \begin{bmatrix} \varepsilon_x^R \\ \varepsilon_y^R \\ \frac{\gamma_{xy}^R}{2} \end{bmatrix}_K \tag{35}$$

2.3 Failure criteria for laminated composites

One of the goals of this study is to maximize the failure pressure of composite cylinders using different criteria to predict pressure failure. We use the Tsai–Wu (Akbulut and Sonmez 2011) and maximum stress (Camanho 2002) criteria to analyze the failure of laminated composite materials. The Tsai–Wu failure condition for the two-dimensional stress state considered here, is

$$\begin{aligned} &\frac{\sigma_1^2}{\sigma_{1T}^U \left|\sigma_{1C}^U\right|} + \frac{\sigma_2^2}{\sigma_{2T}^U \left|\sigma_{2C}^U\right|} + \frac{\tau_{12}^2}{\tau_{12}^{U2}} + \frac{\sigma_1 \sigma_2}{\sqrt{\sigma_{1T}^U \left|\sigma_{1C}^U\right| \sigma_{2T}^U \left|\sigma_{2C}^U\right|}} \\ &+ \left(\frac{1}{\sigma_{1T}^U} - \frac{1}{\left|\sigma_{1c}^U\right|}\right)\sigma_1 + \left(\frac{1}{\sigma_{2T}^U} - \frac{1}{\left|\sigma_{2c}^U\right|}\right)\sigma_2 \le 1 \end{aligned} \tag{36}$$

The expression on the left side of Eq. (36) refers to the failure index. When its value is below 1.0, the structure remains intact; the closer it approaches zero, the higher the safety margin of the laminate. This study employs a safety factor to determine the pressure failure of the cylinder. The safety factor for each lamina SF_{tw}^k, based on the Tsai-Wu criterion, is defined as the multiplier of the stress components σ_i at lamina k, which makes the right-hand side of Eq. (36) equal to 1.0.

$$a\left(SF_{tw}^k\right)^2 + b\left(SF_{tw}^k\right) - 1 = 0 \tag{37}$$

where

$$\begin{aligned} a &= \frac{\sigma_1^2}{\sigma_{1T}^U \left|\sigma_{1C}^U\right|} + \frac{\sigma_2^2}{\sigma_{2T}^U \left|\sigma_{2C}^U\right|} + \frac{\tau_{12}^2}{\tau_{12}^{U2}} + \frac{\sigma_1 \sigma_2}{\sqrt{\sigma_{1T}^U \left|\sigma_{1C}^U\right| \sigma_{2T}^U \left|\sigma_{2C}^U\right|}} \\ b &= \left(\frac{1}{\sigma_{1T}^U} - \frac{1}{\left|\sigma_{1c}^U\right|}\right)\sigma_1 + \left(\frac{1}{\sigma_{2T}^U} - \frac{1}{\left|\sigma_{2c}^U\right|}\right)\sigma_2 \end{aligned} \tag{38}$$

The positive root of Eq. (37) provides the safety factor. Since a negative safety factor lacks physical significance, the absolute value of the first root is taken as the actual safety factor. Subsequently, the

minimum value of SF_{tw}^{k} is selected as the laminate's safety factor.

For maximum stress failure criteria when any of the stress ratios exceeds 1, failure is predicted. The conventional maximum stress criterion can be expressed as follows:

$$\begin{aligned} &Fiber: \ \sigma_1 \geq \sigma_{1T}^{U} \, Or \, |\sigma_1| \geq \sigma_{1C}^{U} \\ &Matrix: \ \sigma_2 \geq \sigma_{2T}^{U} \, Or \, |\sigma_2| \geq \sigma_{2C}^{U} \\ &Shear: \ |\tau_{12}| \geq \tau_{12}^{U} \end{aligned} \tag{39}$$

where $\sigma_1, \sigma_2, \tau_{12}$ are local stresses, σ_{1T}^{U} is the axial tensile strength, σ_{2T}^{U} is the Transverse tensile strength, σ_{1C}^{U} is compressive Axial tensile strength, and σ_{2C}^{U} is compressive transverse strength.

2.4 Structural efficiency

The structural efficiency (Lark 1977) analysis will be conducted for each design to facilitate comparison during the final evaluation phase using Eq. (40) the designs with high structural efficiency indicate that the pressure vessel can handle significant pressures with the least amount of material, contributing to better performance, safety, and cost-effectiveness.

$$e = \frac{PV}{W} \tag{40}$$

where e is structural efficiency, P is failure pressure, V is cylinder volume, and W is cylinder weight.

2.5 Genetic algorithm implementation

Applying genetic algorithm operators to a search problem begins by representing potential combinations of variables using bit strings, analogous to chromosomes in biological genetics. Historically, binary coding has been the predominant representation method, where design variables are expressed as bit strings. This approach is straightforward and widely supported, particularly for problems involving discrete or integer-valued parameters. Binary encoding represents solution characteristics through bit strings, enabling efficient execution of crossover and mutation operations. While this approach facilitates rapid genetic operations, it necessitates additional computational steps for binary conversion, with solution accuracy being inherently tied to this transformation process. The bit string configuration is problem-dependent, but this encoding method demonstrates limitations for certain engineering applications due to two key factors: epistasis (gene interaction effects) and non-intuitive mapping of real-world parameters. These constraints make binary representation unsuitable for design problems requiring direct physical parameter manipulation (Katoch et al. 2021). In this study, natural coding was adopted in the genetic algorithm implementation to represent discrete ply orientations directly, where the gene closely resembles the stacking sequence. As an illustration, the stacking sequence $[\pm 45/0_4/90_2]_s$ can be represented as [+45 −45 0 0 90]. While this natural representation simplifies the coding and decoding processes, it necessitates more specialized programming tailored to the specific set of orientations utilized (Gürdal 2024). By inverting the fitness function (e.g., minimizing the negative of a function for maximization), GAs can easily switch between maximization and minimization without changing the core algorithm, reducing complexity and potential errors. For instance, consider the minimization problem.

$$\begin{aligned} &\text{Minimize} \\ &-f(\boldsymbol{x}), \ \boldsymbol{x} = \{x_1, x_2, x_3, \ldots\ldots\ldots\ldots x_n\} \end{aligned} \tag{41}$$

2.6 Initial population

The genetic algorithm initiates by generating an initial population of designs of a size n_s, typically in a random manner. Each individual undergoes evaluation and is assigned a fitness score based on its objective function value and the objective function values of other individuals within the population (Riche 1994).

2.7 Selection and fitness

In genetic algorithms (GAs), the process of selecting individuals for reproduction is a critical aspect influencing the algorithm's performance. Various fitness selection methods exist, each with its unique approach. Proportional selection, often known as Roulette Wheel Selection, assigns probabilities to individuals based on their fitness, resembling a roulette wheel where higher fitness corresponds to a larger slice. Tournament selection involves randomly

selecting subsets of individuals, with the fittest among them chosen for reproduction. Rank-based selection prioritizes individuals based on their ranking rather than absolute fitness values. Stochastic Universal Sampling selects multiple individuals at once using a fixed interval. Boltzmann selection transforms fitness values into probabilities based on the Boltzmann distribution, promoting exploration in the early stages and exploitation later on. Linear ranking selection assigns probabilities linearly based on an individual's rank. The choice of fitness selection method is crucial, impacting the balance between exploration and exploitation and the algorithm's adaptability to different optimization landscapes. Establishing fitness solely on the numerical values of the objective function or augmented function presents a drawback. Toward the conclusion of the optimization process, as the distinctions between competing designs diminish, the selection pressure favoring superior designs weakens, impeding progress. To address this issue, we opt for roulette wheel Rank-based selection, where fitness is determined by the relative rank of designs, after establishing the fitness for all designs within the population, a prevalent approach for selecting parent designs involves simulating a biased roulette wheel. In this simulation, each design is allocated a sector on the roulette wheel, the area of which is proportionate to its fitness. Specifically, if there are n_s designs with fitness values $\varnothing_i, i = 1, ..., n_s$ the i_{th} design occupies a fraction of r_i of the wheel (Gürdal 2024).

$$\emptyset_i = n_s - i + 1 \tag{42}$$

$$r_i = \frac{2\left(n_s - i + 1\right)}{\left(n_s + 1\right)n_s} \tag{43}$$

On the computer, implementing the roulette wheel can be achieved by generating a random number r within the range of zero to one. Subsequently, the i_{th} design is selected if the following condition is achieved:

$$R_{i-1} \le r \le R_i \tag{44}$$

where $R_0 = 0 and\ R_i = \sum_{j=1}^{i} r_i, i = 1, ..., n_s$

2.8 Crossover

The individuals with the highest fitness in the population are afforded the prime opportunity to act as parents and potentially endure into the subsequent generation. The process of reproduction involves the utilization of a recombination operator, commonly known as a crossover, with a specified probability of implementation. The primary goal of crossover is to inherit advantageous traits from organisms within the parent population, generating offspring expected to be better adapted to their environment than their predecessors. Among the widely used implementations of crossover are one-point and two-point crossover. In the former, the chromosome string of each parent organism is randomly split at one point, while in the latter, it is split at two points. Subsequently, fragments from each parent organism are recombined to give rise to a new offspring. However, if we opt for real numbers as the representation of variables, we encounter a contrasting challenge. In this form of representation, each variable's real value is assigned to a specific location in the genetic string. While the binary representation of these real numbers allows crossover to produce offspring with intermediate values of the parent genes, the limitation arises when each real number is represented by a single gene. In such a scenario, the crossover can only reproduce values present in the initial population. While this condition may be acceptable, as the mutation operator, described in the next section, can introduce new values, an alternative solution to this issue involves replacing the conventional crossover with a cross-average crossover (Soremekun 1997; Gürdal 2024). Cross-average crossover known as an adapted form of Average Crossover is employed, where the average value of the first gene in the first chromosome and the last gene in the second chromosome is calculated to produce the corresponding offspring, this process is repeated until genes from both chromosomes have participated in the crossover, generating the complete set of offspring (Delima et al. 2019)

2.9 Mutation

Subsequently, one of the two offspring is randomly selected and subjected to mutation. Mutation, a stochastic operator, is typically applied with a low probability, causing random changes in some genes

within the chromosome. The primary objective of mutation is to safeguard against the complete loss of genetic material. As the impact of selection reduces the variety of alleles for any given gene in the population, chromosomes tend to converge toward the most optimal known chromosome. Alleles linked to less fit individuals often do not get transmitted to the next generation and may disappear from the population, even though they could be essential later in the search for the optimum solution. The challenge arises when, under the influence of selection, the population becomes predominantly uniform, leading to stagnation in the search as crossover loses its capacity to generate novel designs. Therefore, by retaining genetic diversity through mutation, the ability of crossover to discover new beneficial designs is preserved. Additionally, mutation independently uncovers positive features in the design through random exploration. Since mutation is entirely random, its efficacy in directly discovering improved designs diminishes as the best-known design improves (Riche 1994).

3 The mathematical representation of the optimization

The genetic algorithm seeks the optimal stacking sequence and ply angles to maximize failure pressure, in two scenarios: the first one under mechanical loads and the second under both mechanical and thermal loads, subjected to maximum stress and Tsai-Wu failure criteria for problem I. For problems II and III, the first scenario (under mechanical loads) is subjected to maximum stress and Tsai-Wu failure criteria. The second one (under both mechanical and thermal loads) only considers maximum stress failure criteria, because the genetic approach based on Tsai-Wu failure criteria requires more computational power. The variables in this problem are stacking sequence and ply angles, with the upper limit of 90 and the lower limit of -90; the number of plies is constant.

Problem I Problem I explores a non-hybrid composite cylinder composed of a single type of lamina. The materials used are Carbon Epoxy, Glass Epoxy, and Boron Epoxy. The mathematical depiction of the optimization problems for problem I can be articulated as follows:

$$\text{Find}: \left\{\theta_n\right\}_S \ , \ \theta_n \in [-90, 90], mat_n \in \{CE\}, \{GE\}, \{BE\} \text{where}$$

Number of layers n for;

$$\text{Design I} = 52$$

$$\text{Minimize}: -P_{\text{failure}}(x), x = \left\{\theta_1, \theta_2, \theta_3, \ldots\ldots\ldots..\theta_n\right\}_S$$

$$\text{Subjected to}: \text{ maximum stress, Tsai} - \text{Wu failure criteria}$$

Problem II Problem II involves optimizing a two-material hybrid composite cylinder, specifically designed to balance performance and material usage. The genetic algorithm was constrained to ensure an equal 50% distribution between the two selected materials (e.g., Carbon/Glass Epoxy, Boron/Carbon Epoxy, Boron/Glass Epoxy). This constraint was critical to prevent the algorithm from defaulting to the strongest material and producing a non-hybrid design. The mathematical depiction of the optimization problems for problem II can be articulated as follows:

$$\text{Find} \quad : \left\{\theta_n, mat_n\right\}_S, \theta_n \in [-90,90], mat_n \in \{CE, GE\}, \{BE, GE\}, \{BE, CE\} \text{where}$$

Number of layers n for;

$$\text{Design II} \ = 44,$$

$$\text{Minimize}: -P_{\text{failure}}(x),$$

$$x = \left\{\theta_1 mat_1; \theta_2 mat_2; \theta_3 mat_3; \ldots\ldots\ldots..\theta_n mat_n\right\}_S$$

$$\text{Subjected to}: \text{ maximum stress,}$$

$$\text{Tsai} - \text{Wu failure criteria}$$

Problem III Problem III extends the complexity by optimizing a three-material hybrid composite cylinder, ensuring each material (boron, carbon, and glass epoxy) makes up exactly one-third (33%) of the total plies. This strict balancing constraint maintains the hybrid nature while exploring synergies among the three materials. The mathematical depiction of the optimization problems for problem III can be articulated as follows:

$$\text{Find}: \left\{\theta_n, mat_n\right\}_S, \theta_n \in [-90, 90], mat_n \in \{CE, GE, BE\}$$

Where

Number of layers n for;

Design III $= 78$,

Minimize : $-P_{\text{failure}}(x)$,

$x = \{\theta_1 mat_1; \theta_2 mat_2; \theta_3 mat_3; \ldots\ldots\ldots .. \theta_n mat_n\}_S$

Subjected to : maximum stress,

Tsai − Wu failure criteria

where

CE is Carbon Epoxy, GE is Glass Epoxy, and BE is Boron Epoxy.

Geometrical parameters and the material selection related to the design for this study are presented in Tables 1 and 2, respectively.

4 Numerical results and discussion

This study presents a numerical optimization framework for the structural design of composite LPG cylinders using genetic algorithms. The analysis was conducted under both mechanical and thermomechanical loading conditions. The results are significant in several respects, offering new insights into the interplay between laminate configuration, failure criteria, thermal sensitivity, and cost-performance trade-offs.

Table 1 Geometrical parameters of the design problems

Design parameters	Design I	Design II	Design III
Volume (It)	59.6	73.2	92.4
Inner Radius (mm)	128.5	143.53	170.18
Thickness of a ply (mm)	0.125	0.154	0.126
Length (mm)	977	940	789
Number of ply	52	42	78

4.1 Optimum design under mechanical load

Analyzing the initial and final iterations of the optimization process underscores the convergence achieved through optimization. We can illuminate the progression towards convergence by examining the optimal designs obtained at these two stages. This comparative evaluation illuminates the refinement and improvement in design outcomes throughout the optimization process for both GA algorithms for designs I, II, and III, as shown in Fig. 1.

We employed three distinct materials for design I to explore the optimum layup for achieving the highest failure pressure.

For the second design, we conducted an optimization of a hybrid composite cylinder comprising two distinct materials to maximize pressure failure. This optimization was performed using two different algorithms, and the failure pressure was estimated based on the Tsai-Wu criterion and the maximum stress theory. To ensure a truly hybrid laminate, we enforced a constraint for the algorithms to utilize 50% of each material during optimization. Without this constraint, the genetic algorithm would tend to select designs

Table 2 Typical strengths of unidirectional composites and Measured engineering constants (Agarwal et al. 2017)

Performance parameter		Glass /epoxy	Carbon/epoxy T300/N5208	Boron/ epoxy B-4/ N5505
Axial compressive strength	X_c(MPa)	610	1500	2500
Axial tensile strength	X_t (MPa)	1062	1500	1260
Transverse compressive Strength	Y_c(MPa)	118	246	202
Transverse tensile strength	Y_t(MPa)	31	40	61
Shear strength	S(MPa)	71	68	67
Elastic modulus Shear modulus	E_1 (GPa)	38.6	181	204
	E_2 (GPa)	8.27	10.2	18.5
	G_{12}(GPa)	4.14	7.2	5.59
Thermal expansion coefficient	a_1(μ/°C)	8.6	0.02	6.10
	a_2(μ/°C)	22.1	22.5	30.30
Poisson's ratio	υ_{12}	0.26	0.28	0.23
Fiber volume fraction	ν_f	0.45	0.7	0.5
Density	d(g/cm^3)	1.8	1.6	2

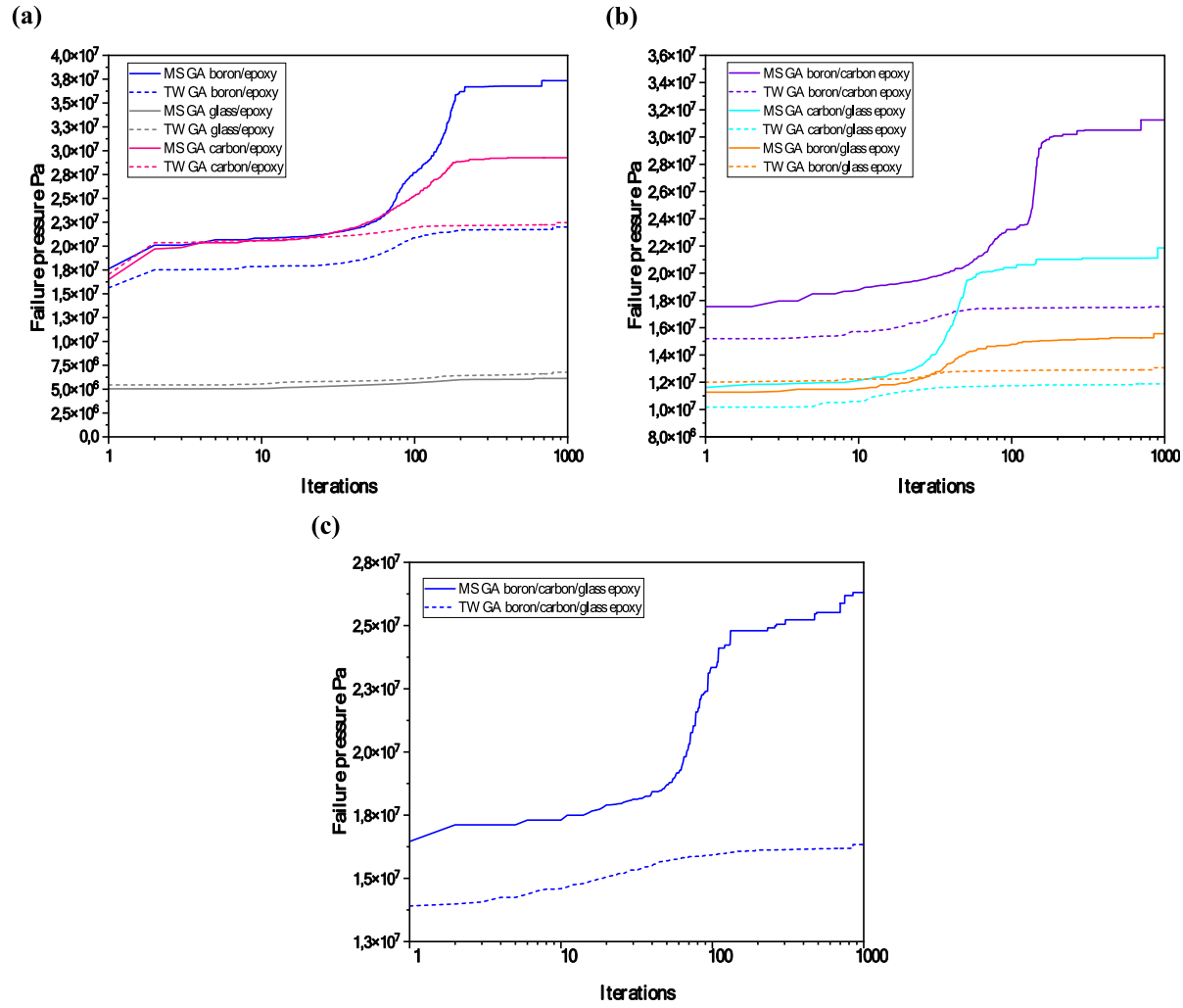


Fig. 1 Convergence of Genetic Algorithm based on Tsai-Wu and Maximum Stress Criteria Optimization across Materials for **a** design I; **b** design II; and **c** design III

solely based on superior material properties, resulting in a non-hybrid laminate.

In the third design, we engaged in optimizing a hybrid composite cylinder constructed from three different materials to enhance its resistance to pressure failure. This optimization process involved the utilization of two distinct algorithms, and the estimation of failure pressure was conducted employing both the Tsai-Wu criterion and the maximum stress theory. A constraint was imposed to ensure the composite cylinder remained truly hybrid, stipulating that each material should constitute 33% of the overall composition during optimization. This constraint was crucial as, without it, the genetic algorithm tended to favor materials with superior properties, resulting in a non-hybrid composition.

The optimal stacking sequence and ply angle for the three designs, along with their estimated pressure failure based on the Tsai-Wu and maximum stress theories, and their structural efficiency, are presented in Table 3.

The investigation reveals a fundamental dependency of optimization outcomes on the selected failure criterion, establishing this choice as a critical design parameter rather than merely a computational consideration. The comparative analysis demonstrates that the Tsai-Wu and Maximum Stress criteria produce substantially different optimal

Table 3 Optimization results of Design I, Design II, and Design III

Design	Design material	GA failure criteria	Optimal layup sequence	$P_{failure}$ (MPa) TW	structural efficiency $\times 10^7 mm$	$P_{failure}$ (MPa) MS	structural efficiency $\times 10^7 mm$
I	Carbon/Epoxy	Tsai-Wu	$[-89/-50/56/-50/-51/-50_3/56_3/-50/56/-50/57/-50_2/56_5/57/-50_2/56]_s$	22.465	1.2530	24.394	1.3606
		Maximum stress	$[51_2/-50/51_2/-50_2/51/-50/51/-50/52_2/-50_2/52_3/-50_2/52/-50/51/-50_3]_s$	18.234	1.0175	29.262	1.6175
	Glass /Epoxy	Tsai-Wu	$[55_3/-53_2/55/57/55/-54/55_2/56/-78/-53/55/56/-53_3/55/-53/55/-53_4]_s$	6.777	0.3359	6.0152	0.2982
		Maximum stress	$[-56_3/48/-56_2/48/-56_5/48/-56_2/48_6/-56/48/-56/48_2]_s$	6.7334	0.3338	6.125	0.3036
	Boron/Epoxy	Tsai-Wu	$[55/-55/56_2/57/56/57/56/-56_2/56/-56/56/-55/56_2/-55/56/-55_2/-57/-55/56_2/-55_2]_s$	22.057	0.9842	36.011	1.6068
		Maximum stress	$[55/-57/55_2/-57/55/-57_3/55/-57_3/55/-57_2/55/-57_2/55/-56/55_5]_s$	21.997	0.9815	37.34	1.6661

Table 3 (continued)

Design	Design material	GA failure criteria	Optimal layup sequence	$P_{failure}$ (MPa) TW	structural efficiency $\times 10^7 mm$	$P_{failure}$ (MPa) MS	structural efficiency $\times 10^7 mm$
II	Carbon/Glass Epoxy	Tsai-Wu	$[-58_c/40_{gl}/52_c/-53_{gl}/-58_{2c}/41_{gl}/52_c/-54_{gl}/58_c/52_{3c}/90_{gl}/-53_{gl}/40_{gl}/41_{gl}/40_{gl}/58_{2c}/40_{gl}]_s$	13.061	0.7665	12.324	0.7232
		Maximum stress	$[-48_c/53_c/-48_{gl}/53_c/55_{gl}/-47_c/-48_{gl}/-47_c/55_{gl}/-48_{gl}/-47_c/53_{2c}/55_{gl}/53_c/-48_{gl}/-47_c/-48_{2gl}/55_{gl}/53_c]_s$	10.594	0.6217	15.565	0.9134
	Boron/Glass Epoxy	Tsai-Wu	$[-48_{gl}/-54_b/-48_{gl}/57_{2b}/56_{gl}/57_b/-54_b/56_{gl}/-54_b/-49_{2gl}/57_b/-48_{gl}/-49_{gl}/57_b/-54_b/57_b/-48_{gl}/-54_b/-48_{gl}]_s$	11.874	0.6349	18.007	0.9629
		Maximum stress	$[-47_b/67_{2gl}/-58_{gl}/-57_{gl}/58_b/67_{gl}/-47_b/69_{gl}/-57_{gl}/58_b/-47_b/68_{gl}/-47_b/58_b/-60_{gl}/58_b/58_{2b}/-47_b/-58_g]_s$	11.341	0.6064	21.859	1.1689
	Boron/Carbon Epoxy	Tsai-Wu	$[-48_c/54_c/-53_{2b}/-48_c/54_c/-48_c/-53_b/-48_c/60_{2b}/54_c/-53_b/60_b/-48_c/60_b/54_c/-53_b/60_b/54_c/60_b]_s$	17.547	0.9644	27.997	1.5389
		Maximum stress	$[-50_b/57_{2c}/58_{2b}/57_c/-50_b/58_b/-49_c/-50_b/58_b/-49_c/60_c/-49_c/57_c/-50_b/58_b/-49_c/58_b/-50_b/-49_c]_s$	17.302	0.9510	31.253	1.7178

Table 3 (continued)

Design	Design material	GA failure criteria	Optimal layup sequence	$P_{failure}$ (MPa) TW	structural efficiency $\times 10^7 mm$	$P_{failure}$ (MPa) MS	structural efficiency $\times 10^7 mm$
III	Boron/Carbon/ Glass Epoxy	Tsai-Wu	$[49_{gl}/-62_b/-51_c/-62_b/49_c/54_{2b}/-46_{gl}/54_b/-62_b/54_b/48_c/49_c/52_{gl}/51_{gl}/48_c/-62_{gl}/-51_c/-62_b/-57_{gl}/-62_b/47_c/46_{gl}/-62_b/54_b/45_{gl}/-49_c/48_c/-49_c/-90_{gl}/-51_c/-49_{gl}/-51_{gl}/54_b/-49_c/-62_b/-48_{gl}/50_{gl}/-50_c]_s$	16.338	0.68166	20.545	0.85718
		Maximum stress	$[-62_b/42_c/-62_b/-59_c/43_b/-61_{gl}/-64_{gl}/-59_c/-67_{gl}/46_{gl}/81_{gl}/42_b/-59_c/-62_b/42_b/-60_c/-59_c/42_c/-64_{gl}/-62_b/44_b/-62_b/41_c/42_{gl}/44_{gl}/-59_c/39_c/42_b/42_c/-62_b/42_c/-62_b/-64_{gl}/44_{gl}/-62_b/74_{gl}/-62_{gl}/-74_{gl}/-59_c]_s$	15.229	0.63539	26.307	1.0976

solutions, with each criterion exhibiting distinct preferences in material selection and generating unique stacking sequence configurations. This criterion-specific behavior results in markedly divergent performance predictions, highlighting that the concept of optimality in composite design is inherently relative to the adopted failure theory. These findings carry significant methodological implications, emphasizing that optimization results must be explicitly contextualized within their failure criterion framework, and suggest the potential value of multi-criterion assessment approaches for comprehensive design evaluation. The study underscores the necessity of carefully aligning failure criterion selection with both performance requirements and safety considerations in engineering applications.

Considering design I, for carbon epoxy, using the Tsai-Wu failure criterion with the genetic algorithm resulted in an optimal layup predicting a failure pressure of 22.465 MPa, whereas the Maximum Stress criterion predicted 24.394 MPa. Conversely, utilizing the Maximum Stress criterion with the genetic algorithm led to a Tsai-Wu-predicted failure pressure of 18.234 MPa and a Maximum Stress theory prediction of 29.262 MPa. This suggests that the optimal layup for Tsai-Wu may not align with that for Maximum Stress. For boron epoxy, we found that, although the optimum layups obtained from the genetic algorithm based on maximum stress and the other one based on

Tai Wu criteria differ, the optimal layups yield failure pressures that are closely aligned within each criterion. However, for glass epoxy, despite differing layup configurations, the results showed relatively close failure pressures, indicating less sensitivity to layup changes in terms of failure pressure. In terms of structural efficiency assessed by the Tsai-Wu failure criteria, the carbon epoxy exhibited the highest efficiency of 1.2530×10^7 mm and a maximum failure pressure of 22.465 MPa, determined by a genetic algorithm based on the Tsai-Wu criterion as the best design. Conversely, based on the maximum stress failure theory, the boron epoxy demonstrated the highest structural efficiency of 1.6661×10^7 mm and a maximum failure pressure of 37.34 MPa, identified by a genetic algorithm based on the maximum stress criterion as the best design.

Considering design II, the findings reveal that, according to the Tsai-Wu criterion, the top-performing design considering structural efficiency was a hybrid cylinder composed of boron epoxy and carbon epoxy materials, yielding a pressure failure of 17.547 MPa and a structural efficiency of 0.9644×10^7 mm identified by genetic algorithm based on the Tsai-Wu criterion. Similarly, for the maximum stress criterion, the top-performing design was the boron epoxy and carbon epoxy hybrid cylinder, with pressure failure of 31.253 MPa and a structural efficiency of 1.7178×10^7 mm identified by a genetic algorithm based on the maximum stress criterion. Conversely, according to the Tsai-Wu criterion, boron glass epoxy was the suboptimal design, with pressure failure estimated at 11.341 MPa and a structural efficiency of 0.6064×10^7 mm identified by genetic algorithm based on the maximum stress criterion. In contrast, according to the maximum stress criterion, the carbon glass epoxy was the suboptimal design with pressure failure estimated at 12.324 MPa and a structural efficiency of 0.7232×10^7 mm identified by the genetic algorithm based on the Tsai-Wu criterion. Notably, while both genetic algorithms favored the boron carbon epoxy hybrid as the superior design, differences emerged in their selection of suboptimal configurations. This observation suggests a potential misalignment between the optimal layup configurations identified by the Tsai-Wu criterion GA and those identified by the Maximum Stress criterion GA. It's also worth highlighting that there exists a substantial disparity in the failure pressure estimates derived from the Tsai-Wu criterion and the maximum stress theory for the same optimal layup.

Finally, for design III, the outcomes reveal variations in the optimal layup and corresponding failure pressures when employing the genetic algorithm. Specifically, for the Tsai-Wu-based genetic algorithm optimum layup, the predicted pressure failure according to the maximum stress theory was 20.54 MPa, and the structural efficiency was 0.85718×10^7 mm, whereas for the Tsai-Wu failure criteria, the failure pressure and structural efficiency were 16.33 MPa and 0.68166×10^7 mm, respectively. Conversely, for the maximum stress-based genetic algorithm optimum layup, the pressure failure estimated based on the Tsai-Wu criterion was 15.30 MPa and the structural efficiency was 0.63539×10^7 mm, while the failure pressure and structural efficiency were 26.3 MPa and 1.0976×10^7 mm, respectively, for the maximum stress theory.

Table 4 presents a comparative analysis of normalized failure pressures for various composite configurations, evaluated using the Tsai-Wu and Maximum Stress failure criteria. The results clearly demonstrate the superior failure resistance of high-performance fiber composites relative to the baseline material. Hybrid designs, particularly those combining boron and carbon fibers, show notable improvements, suggesting beneficial interactions between constituent fibers. The three-phase hybrid offers a balanced performance, potentially enhancing other structural attributes. Differences observed between failure criteria highlight the importance of criterion selection in composite design assessment.

A comparative analysis was conducted to determine the most appropriate material choice for three different designs, taking into account the structural efficiency of each. The three designs with the highest structural efficiency will be compared to identify the optimal one, utilizing both the Tsai-Wu criterion and maximum stress considerations as shown in Fig. 2.

According to the Tsai-Wu criterion, the design exhibiting the utmost structural efficiency was the design I made of carbon epoxy, boasting a remarkable structural efficiency rating of 1.2530×10^7 mm. Conversely, based on the maximum stress criterion, the design showcasing the highest structural efficiency was design II, a hybrid cylinder made of boron carbon epoxy materials, registering a structural efficiency of 1.7178×10^7 mm. The results emphasize the

Table 4 Normalized values for failure pressure, using Glass/Epoxy as the baseline

Design	Design material	GA failure criteria	Normalized $P_{failure}$ (MPa) TW	Normalized $P_{failure}$ (MPa) MS
I	Carbon/Epoxy	Tsai-Wu	3.315	4.0554
		Maximum stress	2.7908	4.7774
	Glass /Epoxy (**Baseline**)	Tsai-Wu	1	1
		Maximum stress	1	1
	Boron/Epoxy	Tsai-Wu	3.2546	5.9866
		Maximum stress	3.2668	6.0963
II	Carbon/Glass Epoxy	Tsai-Wu	1.9272	2.0488
		Maximum stress	1.5733	2.541
	Boron/Glass Epoxy	Tsai-Wu	1.7521	3
		Maximum stress	1.6842	3.57
	Boron/Carbon Epoxy	Tsai-Wu	2.5892	4.65
		Maximum stress	2.5695	5.1
III	Boron/Carbon /Glass Epoxy	Tsai-Wu	2.4108	3.415
		Maximum stress	2.2617	4.3

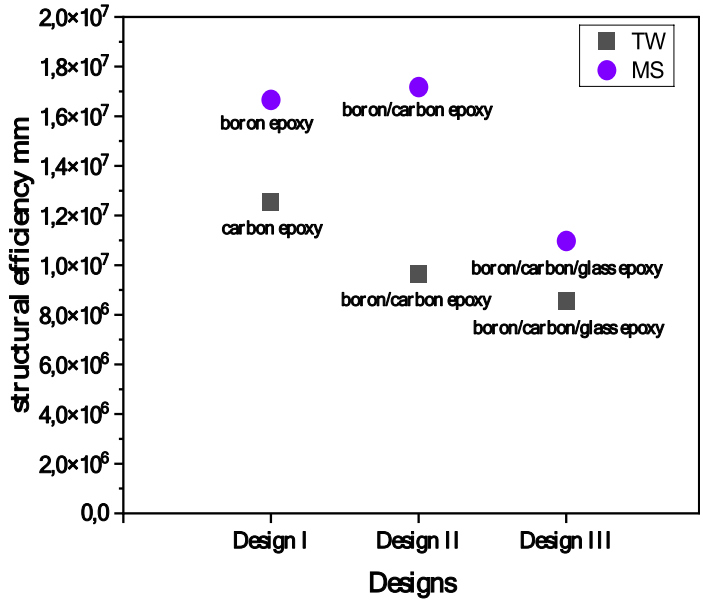


Fig. 2 Design Comparison Based on Tsai-Wu and Max. Stress Criterion: Evaluation of Designs I, II, and III

importance of examining various criteria in assessing the structural efficiency of composite material designs, thus aiding in determining the optimal material choice.

4.2 Cost-effectiveness assessment of optimized composite cylinder designs

In the optimization of composite pressure vessels, especially for applications such as LPG storage, both structural performance and economic viability must be considered. While advanced hybrid laminates can offer improved mechanical characteristics, their cost often limits practical implementation. To guide

material selection, a cost-per-unit structural efficiency metric provides a clear basis for comparing design alternatives. This section evaluates the best-performing configurations across three optimized composite cylinder designs using the Tsai-Wu and Maximum Stress failure criteria, focusing on identifying the most cost-effective solution for real-world applications.

Tables 5 and 6 highlight the critical role of raw material pricing and its impact on the total cost of composite cylinder designs. The cost disparity is substantial: E-glass at \$0.38/kg, carbon fiber at \$40/kg, and boron fiber at \$3834/kg. This difference underscores the importance of cost-performance trade-offs, as boron's superior mechanical properties come with extreme economic penalties.

At the design level, Design I (carbon/epoxy) offers the best balance, costing \$423 while delivering high structural efficiency. Conversely, the boron/epoxy version of the same design reaches \$36,115, making it cost-prohibitive despite excellent strength. Hybrid configurations in Design II show that carbon/glass epoxy, at \$328, achieves a reasonable compromise between performance and affordability, while boron-based hybrids exceed \$20,000 in cost.

Design III, with a three-material hybrid, further illustrates the financial weight of combining high-cost reinforcements, totaling \$22,464. These findings clearly suggest that carbon/epoxy is the most cost-effective choice, and that incorporating expensive fibers like boron should be reserved for highly specialized applications. Future optimization should consider not only mechanical performance but also cost-efficiency and scalability for real-world adoption.

Based on the summarized data from Table 7, it is evident that Design I using Carbon/Epoxy under the Maximum Stress criterion offers the most favorable cost-to-performance ratio, with a structural

Table 5 Raw Materials Approximate Price Per kg

Material	Approximate price per kg	Source
Fiberglass (E-glass)	~\$0.38	Skywell Composite Technology Co., Ltd
Carbon Fiber (T300)	~\$40.00	Skywell Composite Technology Co., Ltd
Boron fiber (B-4)	~\$3834.00	Specialty Materials Inc
Epoxy	~\$37.92	Westlake Epoxy Germany

Table 6 Design Materials approximate price per kg

Design	Material combo	Total volume (m^3)	Fiber volume (m^3)	Fiber density (g/cm^3)	Epoxy volume	Epoxy density (g/cm^3)	Total cost fiber and matrix (USD)
I	Carbon/Epoxy	0.0067	0.0047	1.77	0.002	1.2	\$423
I	Glass/Epoxy	0.0067	0.0030	2.54	0.0037	1.2	\$171.26
I	Boron/Epoxy	0.0067	0.00335	2.8	0.00335	1.2	\$36,115.36
II	Carbon/Glass Hybrid 50%	0.0074	0.00259[a] 0.001665[b]	1.77[a] 2.54[b]	0.003145	1.2	\$328.08
II	Boron/Glass Hybrid	0.0074	0.00185[c] 0.001665[b]	2.8[c] 2.54[b]	0.003885	1.2	\$20,038.51
II	Boron/Carbon Hybrid	0.0074	0.00185[c] 0.00259[a]	2.8[c] 1.77[a]	0.00296	1.2	\$20,178.18
III	B/C/G Hybrid (33% each)	0.0123	0.00205[c] 0.00287[a] 0.001845[b]	2.8[c] 1.77[a] 2.54[b]	0.005535	1.2	\$22,464.00

[a]Carbon fiber

[b]Boron fiber

[c]Glass fiber

Table 7 Best Cost per Unit Efficiency For Designs I, II, and III

Design	Criterion	Best material	Structural efficiency ($\times 10^7$ mm)	Cost USD)	Cost per unit efficiency (USD / 10^7 mm)
I	Tsai-Wu	Carbon/Epoxy	1.2530	423	337.5
I	Max Stress	Carbon/Epoxy	1.6175	423	261.51
II	Tsai-Wu	Carbon/Glass Epoxy	0.9644	328.08	428.1
II	Max Stress	Carbon/Glass Epoxy	1.7178	328.08	359.2
III	Tsai-Wu	B/C/G Hybrid (33% each)	0.6817	22,464.00	32,954.9
III	Max Stress	B/C/G Hybrid (33% each)	1.0976	22,464.00	20,466.6

efficiency of 1.6175×10^7 mm and a cost per unit efficiency of just 261.51 USD per 10^7 mm. This makes it the most economically and structurally efficient choice among all configurations.

In contrast, Design III, particularly under the Tsai-Wu criterion, exhibits an extremely high cost per unit efficiency—over 32,000 USD per 10^7 mm—highlighting the impracticality of such complex, high-cost hybrid designs unless justified by highly specialized performance demands.

Design II's carbon/glass epoxy hybrid offers moderate efficiency at a relatively low cost, but it does not surpass the performance or cost-effectiveness of Design I. Overall, the findings underscore that a well-optimized, single-material composite (carbon/epoxy) can outperform more complex hybrid laminates in both structural efficiency and affordability, especially when guided by targeted failure criteria like Maximum Stress.

4.3 Optimum design under combined mechanical and thermal load

The investigation reveals that thermomechanical loading conditions fundamentally alter the optimization landscape for composite pressure vessels, introducing critical temperature-dependent constraints on achievable performance. The analysis demonstrates a pronounced sensitivity of optimal configurations to thermal variations, with distinct behavioral regimes emerging across different temperature ranges. Notably, the study identifies a narrow thermal operating window where multiple viable stacking sequences exist, beyond which only simplified, suboptimal layups remain feasible.

In this section, we explored the most effective configurations for design I, design II, and design III across various materials. This involved finding the optimal layup in the temperature fluctuation range of − 100–100 °C through the use of a genetic algorithm. For design I, we applied both genetic algorithms based on Tsai-Wu and maximum stress. We exclusively used the genetic algorithm based on maximum stress for designs II and III. The Tsai-Wu genetic algorithm proved to be considerably slower. Optimization is required twice the time of the maximum stress-based genetic algorithm. The results are shown in Fig. 3 for Design I, Fig. 4 for Design II, and Fig. 5 for Design III.

Our results demonstrate that the carbon epoxy design has multiple optimum layups in the temperature range of -0.2 ˚C to 0.5 ˚C. Outside of this range, however, only one optimal design emerged, exhibiting a failure pressure of 4 MPa. The stacking sequence for this design was determined to be $[90_{26}]_s$.

For glass epoxy, our findings indicate that the glass epoxy design exhibits multiple optimal layups within the temperature range of − 0.2–1 °C, outside of this range, only one optimal design emerged, showcasing a failure pressure of 3.2 MPa. The stacking sequence for this design was determined to be $[90_{26}]_s$. Furthermore, it is important to highlight that there was a significant exponential increase in failure pressure when the temperature changed by 0.1 °C, reaching approximately 36.58 MPa, compared to 6 MPa in the absence of temperature change. This phenomenon can be elucidated by considering the glass transition temperature of the epoxy material. The glass transition temperature represents the temperature range

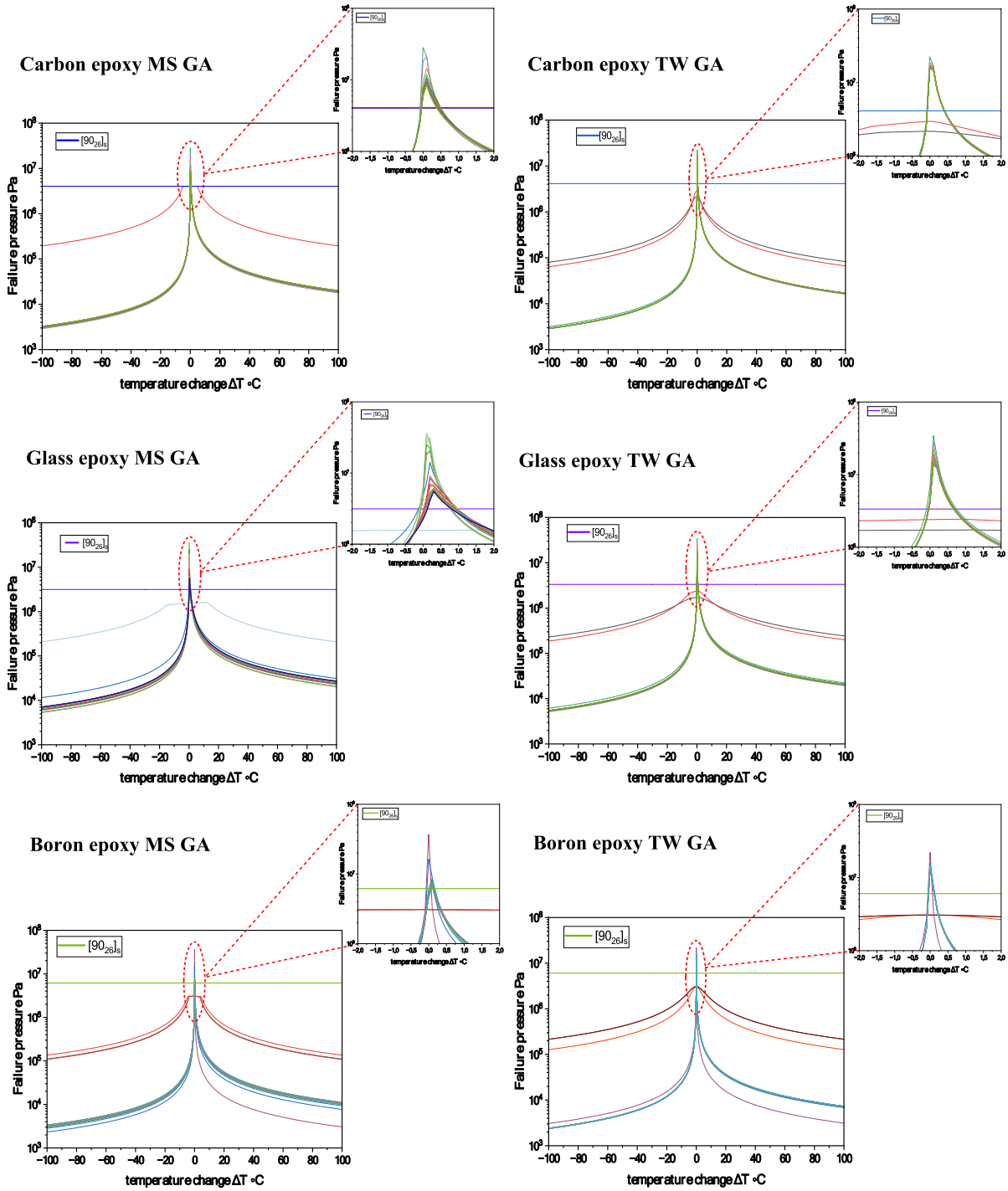


Fig. 3 Optimal design exploration: failure pressure response to variable temperatures via max stress and Tsai-Wu genetic algorithm optimization for design I

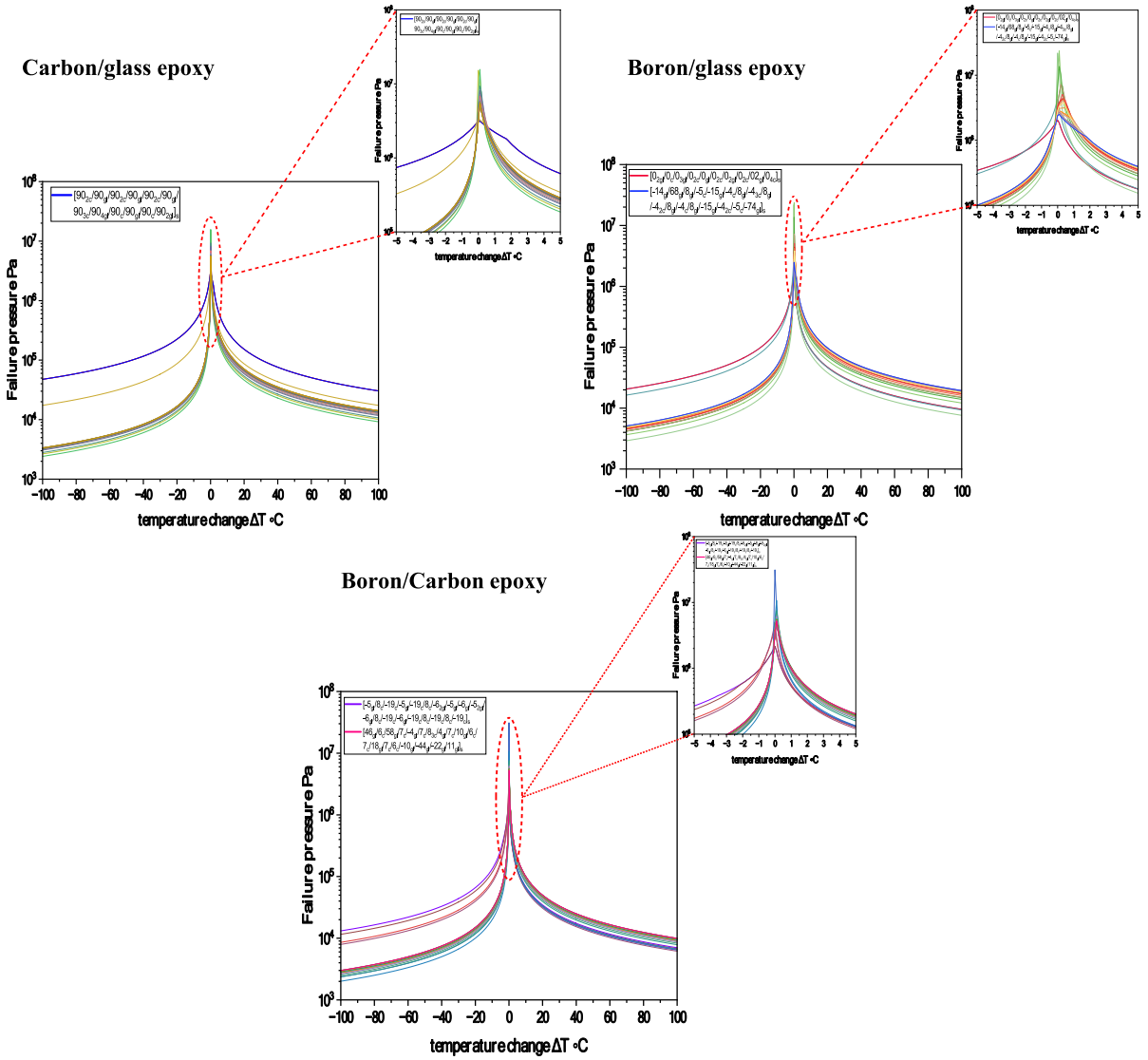


Fig. 4 Optimal design exploration: failure pressure response to variable temperatures via max stress genetic algorithm optimization for design II

at which the polymer undergoes a transition from a rigid, glass-like state to a more pliable, rubbery state.

For boron epoxy, our results demonstrate that the boron epoxy design exhibits multiple optimal layups within the temperature range of −0.2–0.3 °C, outside of this range, only one optimal design emerged, showcasing a failure pressure of 6 MPa. This specific design demonstrates an impressive ability to tolerate substantial fluctuations in temperature compared to other materials during the optimization process. The stacking sequence for this design was determined to be $[90_{26}]_s$.

Considering design II, for the carbon glass epoxy material, it becomes apparent that near zero temperature variation, there exist multiple optimal designs. However, as the temperature deviates from zero on either side, only one design consistently emerges as the optimal choice. Notably, this particular design exhibits a remarkable capability to accommodate significant temperature variations compared to other materials in the optimization process. Moreover, the

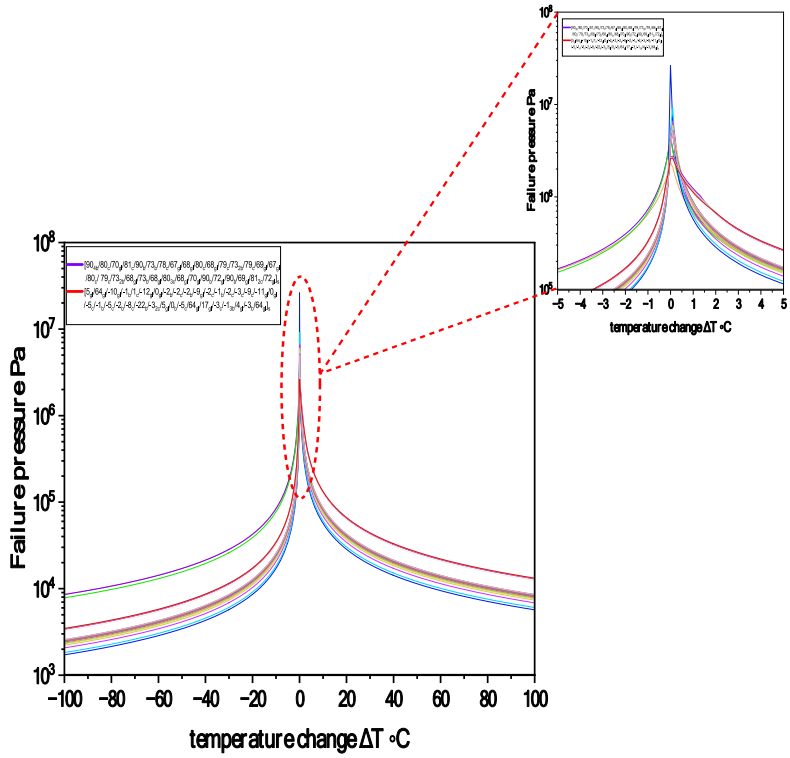


Fig. 5 Optimal design exploration: failure pressure response to variable temperatures via max stress genetic algorithm optimization for design III

optimal configuration of this design involves a stacking sequence of $[90_{2c}\ /90_{gl}\ /90_{2c}\ /90_{gl}\ /90_{2c}\ /90_{gl}\ /90_{3c}\ /90_{4gl}\ /90_{c}\ /90_{gl}\ /90_{c}\ /90_{2gl}]_s$. Similarly, for boron glass epoxy, several optimal designs are evident near zero temperature, with two designs emerging as optimal choices one for positive temperature variations with a layup of $[-14_{gl}\ /68_{gl}\ /8_{gl}\ /-5_{c}\ /-15_{gl}\ /-4_{c}\ /8_{gl}/-4_{3c}\ /8_{gl}\ /-4_{2c}\ /8_{gl}\ /-4_{c}\ /8_{gl}\ /-15_{gl}\ /-4_{2c}\ /-5_{c}\ /-74_{gl}]_s$ and the other for negative temperature changes with a layup of $[0_{2gl}/0_{c}\ /0_{3gl}\ /0_{2c}\ /0_{gl}\ /0_{2c}\ /0_{2gl}\ /0_{2c}\ /0_{2gl}\ /0_{4c}]_s$.

In the case of boron carbon epoxy, multiple optimal designs are observed near zero temperature, with two designs standing out for positive and negative temperature variations. These designs feature layup configurations of $[46_{gl}\ /6_{c}\ /58_{gl}\ /7_{c}\ /-4_{gl}\ /7_{c}\ /8_{3c}\ /4_{gl}\ /7_{c}\ /10_{gl}\ /6_{c}\ /7_{c}\ /18_{gl}\ /7_{c}\ /6_{c}\ /-10_{gl}\ /-44_{gl}\ /-22_{gl}\ /11_{gl}]_s$, and $[-5_{gl}\ /8_{c}\ /-19_{c}\ /-5_{gl}\ /-19_{c}\ /8_{c}\ /-6_{2gl}\ /-5_{gl}\ /-6_{gl}\ /-5_{2gl}\ /-6_{gl}\ /8_{c}\ /-19_{c}\ /-6_{gl}\ /-19_{c}\ /8_{c}\ /-19_{c}\ /8_{c}\ /-19_{c}]_s$ respectively.

For design III, the results illustrate that multiple optimal designs are observed in the vicinity of zero temperature. However, as the temperature deviates from zero, two designs emerge as the most optimal choices: one tailored for positive temperature variations, characterized by a layup configuration of $[5_{gl}\ /64_{gl}\ /-10_{gl}\ /-1_{b}\ /1_{c}\ /-12_{gl}\ /0_{gl}\ /-2_{b}\ /-2_{c}\ /-2_{b}\ /-9_{gl}\ /-2_{c}\ /-1_{b}\ /-2_{c}\ /-3_{c}\ /-9_{c}\ /-11_{gl}\ /0_{gl}\ /-5_{c}\ /-1_{b}\ /-5_{c}\ /-2_{b}\ /-8_{c}\ /-2_{2b}\ /-3_{2c}\ /5_{gl}\ /0_{b}\ /-5_{c}\ /64_{gl}\ /17_{gl}\ /-3_{c}\ /-1_{3b}\ /4_{gl}\ /-3_{b}\ /64_{gl}]_s$, and the other suited for negative temperature fluctuations, featuring a layup arrangement of $[90_{4b}\ /80_{c}\ /70_{gl}\ /81_{c}\ /90_{b}\ /73_{b}\ /78_{c}\ /67_{gl}\ /68_{gl}\ /80_{c}\ /68_{gl}\ /79_{c}\ /73_{2b}\ /79_{c}\ /69_{gl}\ /67_{gl}\ /80_{c}\ /79_{c}\ /73_{2b}\ /68_{gl}\ /73_{b}\ /68_{gl}\ /80_{3c}\ /68_{gl}\ /70_{gl}\ /90_{b}\ /72_{gl}\ /90_{b}\ /69_{gl}\ /81_{2c}/72_{gl}]_s$.

5 Conclusion

This investigation presents a systematic optimization framework for composite pressure vessels employing advanced genetic algorithms, yielding several fundamental insights with significant implications for structural design. The key findings demonstrate:

1. Failure Criterion Dependence: The optimization process exhibits strong sensitivity to the selected failure criterion, with Tsai-Wu and Maximum Stress theories generating fundamentally different optimal configurations. This dependence manifests in both material preference (carbon

versus boron dominance) and stacking sequence characteristics, establishing that optimality must be explicitly contextualized within the chosen failure theory framework.

2. Thermomechanical Behavior: The combined loading analysis reveals critical temperature-dependent performance limitations, identifying distinct operational regimes. A narrow thermal window (−0.2–1 °C) permits multiple viable designs, while extreme conditions necessitate simplified, though suboptimal, configurations. Boron-based composites demonstrate superior thermal stability, though with significant cost penalties.
3. Cost-Performance Tradeoffs: The comprehensive economic assessment establishes carbon/epoxy as the most viable industrial solution, achieving 1.2530×10^{7} mm structural efficiency at $423 material cost. Hybrid configurations offer limited practical advantages when considering both technical and economic factors, while boron-based designs remain prohibitively expensive despite their mechanical benefits.

The optimization process exhibits strong sensitivity to the selected failure criterion, with the Tsai-Wu and Maximum Stress theories generating fundamentally different optimal configurations. For example, design I under mechanical loads, the Tsai-Wu failure criterion based GA finds that the optimal solution for carbon epoxy is $[-89/-50/56/-50/-51/-50_3/56_3/-50/56/-50/57/-50_2/56_5/57/-50_2/56]_s$. In contrast, for the maximum stress failure criterion based GA, the optimal solution is $[51_2/-50/51_2/-50_2/51/-50/51/-50/52_2/-50_2/52_3/-50_2/52/-50/51/-50_3]_s$. The analysis under combined mechanical and thermal loading highlights significant performance constraints driven by temperature variations, uncovering distinct operational regimes. Within a limited thermal range, several viable stacking sequences are achievable; however, outside this window, only simplified—yet less optimal—designs remain feasible. For example, carbon epoxy, both GA identified that $[90_{26}]_s$ is the optimal configuration.

These findings provide:

- A validated methodology for multi-criteria composite optimization,
- Quantitative performance benchmarks under complex loading conditions,
- Practical guidelines for material selection and design configuration,
- Fundamental insights into the thermomechanical behavior of advanced composites.

The study advances pressure vessel design by bridging critical gaps between theoretical optimization and engineering implementation. The demonstrated framework offers substantial improvements over conventional design approaches through its simultaneous consideration of mechanical performance, thermal effects, and economic viability. Future work should focus on experimental validation and extension to multi-objective optimization scenarios, incorporating additional manufacturing constraints.

Author contributions B.M. made the whole study and wrote the main manuscript text. S.B. supervised the whole study. All authors read, reviewed and approved the final manuscript.

Funding Open access funding provided by the Scientific and Technological Research Council of Türkiye (TÜBİTAK). The authors did not receive support from any organization for the submitted work.

Data availability Comprehensive implementation details were provided and the authors are confident that the work if reproducible. For further details and access to the training datasets used in this work, readers are encouraged to contact the authors.

Declarations

Competing interests The authors declare that they have no conflict of interest.

Open Access This article is licensed under a Creative Commons Attribution 4.0 International License, which permits use, sharing, adaptation, distribution and reproduction in any medium or format, as long as you give appropriate credit to the original author(s) and the source, provide a link to the Creative Commons licence, and indicate if changes were made. The images or other third party material in this article are included in the article's Creative Commons licence, unless indicated otherwise in a credit line to the material. If material is not included in the article's Creative Commons licence and your intended use is not permitted by statutory regulation or exceeds the permitted use, you will need to obtain permission directly from the copyright holder. To view a copy of this licence, visit http://creativecommons.org/licenses/by/4.0/.

References

Addou, F.Y., et al.: Effect of porosity distribution on flexural and free vibrational behaviors of laminated composite shell using a novel sinusoidal HSDT. Arch. Civ. Mech. Eng. **24**(2), 102 (2024). https://doi.org/10.1007/s43452-024-00894-w

Agarwal, B. D., Broutman, L. J. and Chandrashekhara, K.: Analysis and performance of fiber composites. John Wiley and Sons, (2017).

Air, A., Shamsuddoha, M., Prusty, B.G.: A review of Type V composite pressure vessels and automated fibre placement based manufacturing. Compos. Part B Eng. **253**, 110573 (2023). https://doi.org/10.1016/j.compositesb.2023.110573

Akbulut, M., Sonmez, F.O.: Design optimization of laminated composites using a new variant of simulated annealing. Comput. Struct. **89**(17), 1712–1724 (2011). https://doi.org/10.1016/j.compstruc.2011.04.007

Attia, A., et al.: Free vibration analysis of thick laminated composite shells using analytical and finite element method. J. Vib. Eng. Technol. vol. 12, (2024). https://doi.org/10.1007/s42417-024-01322-2.

Belbachir, N., Tounsi, A., Al-Osta, M.A.: A new HSDT for buckling and free vibration behavior of cross-ply laminated composite plates resting on elastic foundation. Comput. Concrete. **35**(1), 29 (2025)

Blom, A.W., Stickler, P.B., Gürdal, Z.: Optimization of a composite cylinder under bending by tailoring stiffness properties in circumferential direction. Compos. Part B Eng. **41**(2), 157–165 (2010). https://doi.org/10.1016/j.compositesb.2009.10.004

Camanho, P. P.: Failure criteria for fibre-reinforced polymer composites (2002)

Chandrakar, A.T.: Design and analysis of a composite cylinder for the storage of liquefied gases. Int. J. Sci. Res. Develop. **5**(3), 2321–2613 (2017)

Chattopadhyay, A., Ferreira, J.: Design sensitivity and optimization of composite cylinders. Compos. Eng. **3**(2), 169–179 (1993). https://doi.org/10.1016/0961-9526(93)90040-Q

Chawla, K. K.: Macromechanics of Composites. In: Composite Materials, pp. 347–376. Springer, New York (1998). https://doi.org/10.1007/978-1-4757-2966-5_11.

Chen, M., Zhang, X., Shen, K., Pan, G.: Optimization of composite cylinder shell via a data-driven intelligent optimization algorithm. J. Phys. Conf. Ser. **2181**(1), 012019 (2022). https://doi.org/10.1088/1742-6596/2181/1/012019

Delima, A.J., Sison, A.M., Medina, R.P.: A modified genetic algorithm with a new crossover mating scheme. Indo. J. Electr. Eng. Inf. (IJEEI). **7**(2), 165–181 (2019). https://doi.org/10.11591/ijeei.v7i2.1047

Gürdal, Z., Haftka, R. T., Hajela, P.: Design and optimization of laminated composite materials. John Wiley & Sons, (1999). Available: https://www.wiley.com/en-us/Design+and+Optimization+of+Laminated+Composite+Materials-p-9780471252764

Hwang, H.Y.: A review of generative AI applications for composite materials and composite structure design. JMST Adv. (2025). https://doi.org/10.1007/s42791-025-00095-3

Hyer, M. W. and White, S. R.: Stress Analysis of Fiber-reinforced Composite Materials. DEStech Publications, Inc (2009)

Jones, B. H. and Li, M. C.: Liner-less tanks for space application—design and manufacturing considerations (2003)

Katoch, S., Chauhan, S.S., Kumar, V.: A review on genetic algorithm: past, present, and future. Multimed. Tools Appl. **80**(5), 8091–8126 (2021). https://doi.org/10.1007/s11042-020-10139-6

Kaw, A. K.: Mechanics of composite materials, 2. ed. In: Mechanical Engineering Series, no. 29. CRC Taylor & Francis, Boca Raton, FL (2006)

Lark, R. F.: Recent advances in lightweight, filament-wound composite pressure vessel technology, presented at the 1977 Energy Conf., Houston, TX (1977). Accessed: Jun. 27, 2024. [Online]. Available: https://ntrs.nasa.gov/citations/19770026321

Liu, B., Haftka, R.T., Akgün, M.A., Todoroki, A.: Permutation genetic algorithm for stacking sequence design of composite laminates. Comput. Methods Appl. Mech. Eng. **186**(2), 357–372 (2000). https://doi.org/10.1016/S0045-7825(99)90391-2

Mallick, P. K.: Fiber-reinforced composites: materials, manufacturing, and design, 3rd ed., [Expanded and rev. Ed.]. CRC Press, Boca Raton, FL (2008).

Mallick, K., Cronin,J., Fabian, K. and Tupper, M.: Microcrack resistant polymers enabling lightweight composite hydrogen storage vessels. In: Wicks, G., Simon, J., Zidan, R., Lara-Curzio, E., Adams, T., Zayas, J., Karkamkar, A., Sindelar, R., and Garcia-Diaz, B. (Eds.) Ceramic Transactions Series, 1st ed., vol. 224, pp. 91–98. Wiley (2010). https://doi.org/10.1002/9781118019467.ch9.

Mallikarjun, J., Naga, S. T. P., Bharadwaj, S. R. G., Sai Jagannadh, N., and Akhil Gupta, J.: Optimization of stacking sequence of composite cylindrical shells using genetic algorithm. Int. J. Mech. Prod. Eng. Res. Dev, vol. 8 (2018). https://doi.org/10.24247/ijmperdjun201822.

Messager, T., Pyrz, M., Gineste, B., Chauchot, P.: Optimal laminations of thin underwater composite cylindrical vessels. Compos. Struct. **58**(4), 529–537 (2002). https://doi.org/10.1016/S0263-8223(02)00162-9

Mikroni, M., Koutsoukis, G., Vlachos, D., Kostopoulos, V., Vavouliotis, A., Trakakis, G., Athinaios, D., Nikolakea, C., Zacharakis, D.: Design, analysis, and testing of a type V composite pressure vessel for hydrogen storage. Polymers **16**(24), 3576 (2024). https://doi.org/10.3390/polym16243576

Mouaici, F., Benyoucef, S., Atmane, H.A., Tounsi, A.: Effect of porosity on vibrational characteristics of non-homogeneous plates using hyperbolic shear deformation theory. Wind Struct. **22**(4), 429–454 (2016)

Nagendra, S., Haftka, R.T., Gurdal, Z.: Stacking sequence optimization of simply supported laminates with stability and strain constraints. AIAA J. **30**(8), 2132–2137 (1992). https://doi.org/10.2514/3.11191

Nedri, K., El Meiche, N., Tounsi, A.: Free Vibration analysis of laminated composite plates resting on elastic foundations by using a refined hyperbolic shear deformation theory. Mech. Compos. Mater. **49**(6), 629–640 (2014). https://doi.org/10.1007/s11029-013-9379-6

Pan, Z., Zhang, L.-W., Liew, K.M.: Adaptive surrogate-based harmony search algorithm for design optimization of variable stiffness composite materials. Comput. Methods Appl. Mech. Eng. **379**, 113754 (2021). https://doi.org/10.1016/j.cma.2021.113754

Pelletier, J.L., Vel, S.S.: Multi-objective optimization of fiber reinforced composite laminates for strength, stiffness and minimal mass. Comput. Struct. **84**(29–30), 2065–2080 (2006). https://doi.org/10.1016/j.compstruc.2006.06.001

Rao, A.R.M., Lakshmi, K.: Multi-objective optimal design of hybrid laminate composite structures using scatter search. J. Compos. Mater. **43**(20), 2157–2182 (2009). https://doi.org/10.1177/0021998309339221

Le Riche, R.: Optimization of composite structures by genetic algorithms, (1994). Accessed: Feb. 12, 2024. [Online]. Available: http://hdl.handle.net/10919/38270

Riche, R.L., Haftka, R.T.: Optimization of laminate stacking sequence for buckling load maximization by genetic algorithm. AIAA J. **31**(5), 951–956 (1993). https://doi.org/10.2514/3.11710

Saidi, H., Tounsi, A., Bourada, F., Bousahla, A.A., Tounsi, A., Al-Juboori, F.I.: Vibrational behavior of porous composite laminated plates using four unknown integral shear deformation theory. Steel Compos. Struct. **52**(3), 249–271 (2024)

Soremekun, G. A.: Genetic algorithms for composite laminate design and optimization. PhD Thesis, Virginia Tech (1997). Accessed: Jun. 28, 2024. [Online]. Available: https://vtechworks.lib.vt.edu/items/bdc060eb-1762-40e0-9005-4ee6781db7e0

Soremekun, G., Gürdal, Z., Haftka, R.T., Watson, L.T.: Composite laminate design optimization by genetic algorithm with generalized elitist selection. Comput. Struct. **79**(2), 131–143 (2001). https://doi.org/10.1016/S0045-7949(00)00125-5

Thomas, B., Lycksam, H., Forsberg, F., Oksman, K.: Morphological and dynamic mechanical properties of biobased epoxy composites with anisotropic, green carbon aerogels as reinforcement. Compos. Part B Eng. **290**, 111962 (2025). https://doi.org/10.1016/j.compositesb.2024.111962

Tsai, S. W.: Mechanics of Composite Materials, Part 1 – Introduction. (1966). Accessed: Jun. 28, 2024. [Online]. Available: https://www.academia.edu/93661718/Mechanics_of_Composite_Materials_Part_1_Introduction

Youzera, H., Ali, A., Meftah, S.A., Tounsi, A., Hussain, M.: Nonlinear damping and forced vibration analysis of laminated composite plates with composite viscoelastic core layer. Steel Composite Struct., Int. J. **1**, 91–104 (2022)

Publisher's Note Springer Nature remains neutral with regard to jurisdictional claims in published maps and institutional affiliations.